



## **Final Draft of the original manuscript**

Gnedenkov, A.; Mei, D.; Lamaka, S.; Sinebryukhov, S.; Mashtalyar, D.; Vyaliy, I.; Zheludkevich, M.; Gnedenkov, S.:

**Localized currents and pH distribution studied during corrosion of MA8 Mg alloy in the cell culture medium.**

In: Corrosion Science. Vol. 170 (2020) 108689.

First published online by Elsevier: 21.04.2020

<https://dx.doi.org/10.1016/j.corsci.2020.108689>

# Localized currents and pH distribution studied during corrosion of MA8 Mg alloy in the cell culture medium

A.S. Gnedenkov<sup>a,□</sup>, D. Mei<sup>b</sup>, S.V. Lamaka<sup>b</sup>, S.L. Sinebryukhov<sup>a</sup>, D.V. Mashtalyar<sup>a,c</sup>, I.E. Vyalii<sup>a</sup>, M.L. Zheludkevich<sup>b,d</sup>, S.V. Gnedenkov<sup>a,c</sup>

<sup>a</sup> *Institute of Chemistry of FEB RAS, 159 Pr. 100-letiya Vladivostoka, Vladivostok, 690022, Russia*

<sup>b</sup> *Magnesium Innovation Centre – MagIC, Institute of Materials Research, Helmholtz-Zentrum Geesthacht (HZG), 21502 Geesthacht, Germany*

<sup>c</sup> *Far Eastern Federal University, 8 Sukhanova St., Vladivostok, 690950, Russia*

<sup>d</sup> *Institute for Materials Science, Faculty of Engineering, Kiel University, Kiel, Germany*

## Abstract

Electrochemical behaviour of MA8 magnesium alloy in minimum essential medium (MEM) and 0.83 wt. % NaCl solution is compared using SVET, local pH measurements and hydrogen evolution tests. Corrosion products formed on the alloy surfaces are characterized using XRD and SEM-EDX analysis. Potential by-products of cells and bacteria activities increase the sample activity in MEM at the initial stage of material immersion. Hydrogen evolution rate is higher for samples in NaCl solution in comparison with MEM. Formation of partially protective magnesium-substituted hydroxyapatite stabilizes the local pH of MEM below 9.0 and does not allow to increase the pH during corrosion.

---

**Keywords:** A. Magnesium; A. Alloy; B. SEM; B. XRD, C. Passive films

## 1. Introduction

Magnesium is very light metal, which possesses many useful properties such as high strength to weight ratio and good electrical and thermal conductivity [1–3]. Magnesium and its alloys can be used in implant surgery as biodegradable materials [4–16]. The main shortcoming of these materials is they often do not possess sufficient corrosion resistance, since the magnesium is highly electrochemically active metal. This disadvantage of the magnesium-based materials can be turned to an advantage, since the corrosion activity combined with the biocompatibility of the Mg alloys can promote the biodegradation process, which makes these alloys good candidates to be used as a degradable biomaterial. The state-of-the-art on biodegradable materials based on Mg corrosion has been reviewed by Witte et al. [17]. In the recent review [18] Virtanen et al. illustrated the challenges in understanding and controlling the corrosion behaviour of Mg alloys regarding their use as bioresorbable implants in medicine.

---

□ – Corresponding author. Tel: +8 4232215284; fax: +8 4232312590;  
E-mail: [asg17@mail.com](mailto:asg17@mail.com) (A.S. Gnedenkov).

The study of the magnesium alloy corrosion in different media is of great interest, especially in the field of biomedicine, since understanding of the process occurring on the surface of magnesium-based implant is essential to efficient and safe use of this material as a bioresorbable one. Taking into account the rapid degradation process of Mg alloys in chloride-containing solutions and very complex composition of the human body media, it is worth to study the mechanism and kinetics of the Mg alloys corrosion in solutions, which closely resemble that of human body fluids. A number of cell culture media are commercially available. They differ in composition: MEM – minimum essential medium (or Eagle's minimum essential medium); DMEM (or D-MEM) – Dulbecco's modified Eagle's Medium,  $\alpha$ -MEM – minimum essential medium Eagle, alpha modification [19,20]. Many research groups used these media to investigate the features of the magnesium biocorrosion and to reveal the effect of physiological solution composition on Mg and its alloy degradation. Wagener et al. [21] established that immersion of magnesium (99.9 % purity) in DMEM can lead to the formation of a corrosion layer consisting mainly of calcium phosphate compounds that can enhance corrosion resistance of magnesium. However, proteins adsorbed on the surface hinder the formation of a calcium phosphate layer. Yang et al. [22] used SBF (simulated body fluid) solution for immersion of ZK60 alloy samples with and without nano-hydroxyapatite coatings to examine the long-term *in vitro* degradation behaviour. It was established [22] that coating obtained by a hydrothermal deposition method on ZK60 samples, significantly improved corrosion resistance of the material and protected it against rapid degradation. Based on XRD, EDX and FT-IR characterizations, Rettig et al. [23] established that precipitate layers formed in modified SBF solution on a rare-earth containing Mg alloy consisted of amorphous, hydrated, carbonated (Ca, Mg)-phosphate. It was found [24] that during Mg alloy immersion in albumin-containing SBF solution albumin adsorption suppresses early-stage corrosion due to low chelation rate. However, the chelation effect gradually becomes more significant than adsorption, which leads to the breakdown of the protein layer, and corrosion acceleration. In [25] Mei et al. studied the influence of individual ions in SBF on the corrosion process of commercially pure magnesium. The critical impact of the synergistic combination of  $\text{Ca}^{2+}$ ,  $\text{Mg}^{2+}$ ,  $\text{HPO}_4^{2-}$  and  $\text{HCO}_3^-$  causes growth of the partially protective film of hydroxyapatite-like compounds on top of  $\text{MgO}/\text{Mg}(\text{OH})_2$  layer which becomes thicker in time. If at least one of these components is lacking, the hydroxyapatite-like compounds do not form which is manifested by higher magnesium degradation rates. Furthermore, the influence of MEM components, solely or combined in groups of amino acids, vitamins, saccharides, and Krebs's cycle compounds, has also been explored [26]. None of the listed components critically affected the degradation rate of Mg, most probably owing to the low concentrations of these components, typically in the range of 0.1 to 1 mM.

In [27] Bowen et al examined the composition of corrosion products formed on commercial purity Mg explanted from rats' arteries after 30 days of degradation. They found a duplex structure of corrosion products comprising magnesium-substituted hydroxyapatite in the inner layer that later transformed into a carbonate-substituted hydroxyapatite. In [28] Keim et al.

detected similar chemical composition of the corrosion product layers after immersion in SBF and cell culture medium, higher carbon content in the surface layer formed in culture medium was found, which can be related to surface “passivation” by formation of insoluble Mg-carbonate layers [29,30]. All the cited works studied the behaviour of magnesium alloys in various biological solutions. However, based on the analysis of the literature, it is rather difficult to compare these results since they were obtained under largely varying conditions. In the recent review [4] Virtanen compared the protective properties of the surface layers formed on Mg alloys in SBF and DMEM and established the chemical composition of the corrosion product layers. Virtanen also summarized the influence of specific biological environments on the corrosion behaviour of Mg alloys, and discussed some aspects of interactions between corroding Mg surfaces and cells [4]. Nevertheless, there are still open questions on understanding the mechanism of Mg corrosion in cell culture medium. Nowadays, the base of theoretical and experimental tools in the field of electrochemistry is of very high level, which makes it possible to study, understand and control the corrosion processes as well as the biodegradation of magnesium alloys. Local electrochemical methods of surface investigation like Scanning Vibrating Electrode Technique (SVET) and Scanning Ion-Selective Electrode Technique (SIET), according to the previous results of works [31–47], are prospective tools to study the mechanism and kinetics of the corrosion process of metals and alloys. In [32] Lamaka et al. showed for the first time applicability of local pH and  $Mg^{2+}$  measurements in mapping mode near the surface of coated Mg alloy. Córdoba et al. [48] used SVET and SIET to study the localized corrosion phenomena and localized pH evolution of silane-TiO<sub>2</sub> coated AZ31 and ZE41 Mg alloys intended for biomedical applications. Ivanou et al. [49] used SVET to investigate the performance of complex PEO-coatings on ZE41 magnesium alloy in conditions simulating coating damage. Izquierdo et al. [50] used Scanning Electrochemical Microscopy (SECM) in potentiometric operation for the local characterization of the electrochemical behaviour of magnesium-based materials using pH-sensitive and  $Mg^{2+}$ -ion-selective electrodes. Jamali et al. [51] employed different modes of SECM such as surface generation/tip collection, amperometry, AC-SECM and potentiometry to characterize the active/passive domains, hydrogen evolution and local pH on a corroding surface of AZ31 in HEPES stabilized simulated body fluid. Mareci et al. [52] employed SECM technique to characterize the pH variations occurring during the vigorous degradation of MgCa alloys in Ringer's physiological solution with high spatial resolution. Tefashe et al. [53] used high resolution electron microscopy, SVET, SECM amperometric detection of H<sub>2</sub> fluxes, potentiometric SECM detection of local pH and localized potentiodynamic measurements to evaluate the microstructure and corrosion protectiveness of the electrodeposited coating on AZ31B magnesium alloy. Lamaka et al. the first time studied the evolution of local pH in HBSS solution with or without physiological amount of Ca<sup>2+</sup> near the surface of four Mg alloys (potentially relevant for implant applications) [54]. A significant difference in local pH was observed for Mg in simple Hank's solution (near surface pH 9.9–10.5) or Hank's solution modified with 2.5 mM Ca<sup>2+</sup> (pH 7.8–8.5). This effect was explained by the synergy of Ca<sup>2+</sup>,

$\text{HPO}_4^{2-}$ ,  $\text{HCO}_3^-$  and  $\text{Mg}^{2+}$  that stimulate growth of hydroxyapatite-like products on the surface of  $\text{MgO/Mg(OH)}_2$  layer [25,54]. Magnesium corrosion acceleration in the SBF-like electrolytes containing synthetic pH buffers (e.g. TRIS or HEPES) was explained [25,54]. The localized measurements have been proven to be beneficial for the understanding of corrosion mechanism of Mg alloys in inorganic simulated body fluid (like SBF, HBSS), but there are only a few works about localized measurements used in organic-containing simulated body fluids (like cell culture media), which are often used corrosive media for the *in vitro* corrosion tests. Therefore, lack of the detailed information about localized electrochemical behaviour of magnesium-based materials in MEM-like solutions (simulated body fluids, which have the protein composition of mammalian cells) should be removed. Aspects of Mg and its alloys biodegradation, studied on microscale level, must be pointed out and exposed to promote the concept of application of these materials as bioresorbable implants.

Moreover, the capability of carrying out SVET and SIET studies in rather complex biological medium like MEM should be also revealed and established to show all facilities of localized techniques.

This work firstly describes the possibility and procedure of making SVET and local pH measurements in the MEM electrolyte for MA8 Mg alloy [55–61]. To promote Mg alloy application as a bioresorbable implant for osteosynthesis, the presence of the amino acids in the medium is essential. Therefore, MEM was used as one of the test solutions, which simulates a human blood plasma, to show the role of its composition in the corrosion process. To identify the features of processes in a medium containing a large number of organic components, a 0.83% NaCl solution was used as a reference solution. The difference of corrosion process development of the MA8 Mg alloy in 0.83 % NaCl solution and MEM on a microscale level was established. The importance of this work is connected with necessity of the detailed analysis of the electrochemical behaviour of the biodegradable magnesium alloy in the solution with similar composition to the human body fluids (barring the proteins and cells). As a result of this work, one step forward is made in understanding behaviour of Mg as a biodegradable implant material.

## 2. Experimental

### 2.1. Samples and solutions

In the present work, MA8 magnesium alloy sample with low amount of alloying elements (Table 1) was used for investigation. The composition of the alloy was studied using Optical Emission Spectroscopy (PDA-MF Plus, Shimadzu, Japan). All specimens were mechanically ground for surface standardization using silicon carbide papers with abrasive material grain size decreasing down to 15  $\mu\text{m}$  and, thereafter, polished using Aluminum Oxide Lapping Films (Thorlabs Inc., USA) with the grain size down to 3  $\mu\text{m}$ . Ethanol was used for lubrication at the polishing step. After the polishing, the specimens were rinsed with ethanol and dried in air.

Unification of surface preparation is required for further analysis using the combination of applied methods described below.

MA8 Mg alloy samples were studied either in MEM (# 61100 powder, Gibco<sup>®</sup>, Thermo Fisher Scientific, USA) [62,63], with addition of 2.2 g L<sup>-1</sup> NaHCO<sub>3</sub> [64] (the composition of MEM is summarized in Table 2) or in 0.83 wt. % NaCl solution (Na<sup>+</sup> and Cl<sup>-</sup> concentrations are comparable with MEM and the human blood plasma [19]).

## **2.2. Electrochemical measurements**

In order to investigate the development of the corrosion process on the surface of MA8 magnesium alloy and to study the difference in the corrosion behaviour of Mg alloy in 0.83 % NaCl solution and MEM, the SVET/SIET system (Applicable Electronics, USA) was used.

A Pt–Ir insulated wire (Microprobe Inc.) was used as the SVET probe. The tip of the probe was activated via deposition of a platinum black in platinum chloride plating solution (18 mL deionized H<sub>2</sub>O, 0.2 mL 1 % lead acetate solution – Pb(CH<sub>3</sub>COO)<sub>2</sub>·3H<sub>2</sub>O, 2.0 mL 10 % hexachloroplatinic solution – H<sub>2</sub>PtCl<sub>6</sub>·6H<sub>2</sub>O) in accordance with method developed by Applicable Electronics Inc. [65]. SVET measurements were done with vibrating probe placed 100 ± 5 µm above the surface (this error is usually up to 5 % [41,66,67] and is measured in accordance with the minimal step of the motion system (near 700 nm) and the size of the spherical probe tip, which is positioned at the angle to the surface). This distance (100 µm) was chosen to maximize the signal/noise ratio [41]. Frequencies of probe vibration were 99 Hz (Z-axis) and 160 Hz (X-axis) and the vibration amplitudes (peak-to-peak) were equal to 16 µm (Z-axis) and 17 µm (X-axis). The diameter of the probe tip was 15 µm. The SVET device recorded the vertical (Z) and horizontal (X) components of vibrations. However, only Z-component of the current was taken into account for the calculations and mapping the current density, since the analysis of the X-component is not considered paramount to achieve the goals of this work. For processing the experimental data the vertical (Z) component was used according to the existing practice of studying such objects [41,68–70]. In the case of analysis of more complex objects (for measuring the current distribution in a galvanic couple), the X-axis of vibrations also brings relevant information and additionally is taken into account [71]. The pH-selective microelectrode was used for SIET measurements. Single-barreled glass capillaries (1.5 mm o.d.) were used for pulling capillary with 2.0 ± 0.5 µm diameter of the conic tip by means of the P-97 Flaming/Brown Micropipette Puller (Sutter Instruments Company, USA). Obtained capillaries were silanized in a glass preparation chamber at 205 °C. N, N-dimethyltrimethylsilylamine (200 µL) was a silanizing agent. The tip of micropipettes was filled with a pH selective ionophore-based membrane of the following composition: 0.5 wt.% polyvinylchloride, 9.9 wt.% hydrogen ionophore I – tridodecylamine, 88.9 wt.% 2-nitrophenyloctyl ether and 0.7 wt.% potassium tetrakis (4-chlorophenyl) borate (Selectophore products, Fluka) [32,66,72]. Optical microscope and 3D micromanipulators were used to embed the membrane cocktail into the glass tip. The lengths of the membrane column was 60–70 µm. Capillaries were also back-filled with an inner reference solution (0.01 M KH<sub>2</sub>PO<sub>4</sub> in

0.1 M KCl) and silver chlorinated wire was set into the internal solution to provide the connection.

During SIET measurements, the pH microelectrode was placed at  $40 \pm 5 \mu\text{m}$  above the surface. The distance from the surface to the SVET probe and SIET microelectrode was different, due to their different sensitivities [73]. It was previously studied that the accurate values of local pH can be measured at probe distance to surface in the range of  $50 \mu\text{m}$  [54]. MEM and NaCl solutions with defined pH values were used to calibrate pH-selective microelectrodes according to the Nernst equation. The microelectrodes had a reliable potential in the pH range 5.0–12.5. The linear response slope was  $57.1 \pm 0.5 \text{ mV pH}^{-1}$  in 0.83 % NaCl solution and  $56.0 \pm 0.7 \text{ mV pH}^{-1}$  in MEM.

The Ag/AgCl/0.1 M KCl, 0.01 M  $\text{KH}_2\text{PO}_4$  electrode was an external reference electrode for SIET. To make a quasi-simultaneous SVET/SIET measurements [73] on the magnesium alloy surface the dual-head stage was used to place the microelectrodes. The SVET/SIET tests were operated using LV-4 software (ScienceWares, USA). SVET and SIET microelectrodes were placed at a distance to each other equal to  $(55 \mu\text{m}) - (30 \mu\text{m}) - (60 \mu\text{m})$  in X-Y-Z planes.

The sample area was isolated with beeswax (Sigma-Aldrich, USA, # 243221) for localized measurements. The exposed investigated area of the MA8 magnesium alloy did not exceed  $5.5 \text{ mm}^2$ . The reliability of the obtained results was double-checked on similar specimens. Local current density and pH were mapped on  $42 \times 42$  point grid (1764 data points). MA8 Mg alloy samples were studied in MEM and in 0.83 % NaCl solution under open circuit potential conditions. Optical images of the SVET probe and SIET microelectrode, SEM image of the SVET probe tip, schematic of the SIET microelectrode tip and photo of the isolated surface with electrodes before SVET/SIET tests are shown in Fig. 1.

The development of the corrosion process on the surface of the MA8 magnesium alloy was observed using SVET/SIET methods during samples immersion in the media up to 3 days. SVET/SIET measurements were carried out every hour with several periods of system calibration.

During the test, the solution concentration was maintained to prevent the medium evaporation and provide the stable solution conductivity for SVET measurements. MEM and 0.83 % NaCl solutions were circulated through the SVET/SIET cell by means of two-channel peristaltic pump. This also allowed to replenish the constituents of the electrolyte that get consumed and to support the flow condition found in the human body. The schematic of the solution circulation through the SVET/SIET cell, which shows the direction of the flow is presented in Fig. 2a (MEM was used as an example). The speed of solution circulation was  $1.2 \pm 0.2 \text{ mL min}^{-1}$ . This speed was chosen for the maximum possible approximation to the blood flow in the human body, taking into account the low volume of the SVET/SIET cell and high sensitivities of the electrodes. As found in [54,67] the solution circulation rate in the SVET/SIET cell, created using a peristaltic pump, equal to  $1.5 \text{ mL min}^{-1}$ , allows us to obtain reliable local pH values. In our case, the volume of the solution in the SVET/SIET cell was

around 4 mL (the ratio of the sample surface area to solution volume was 1:70 cm<sup>2</sup> mL<sup>-1</sup>). The complete renewal of the solution in this cell occurred every 3.3 minutes.

Since a high amount of additions presents in MEM (Table 2) it is necessary to find their influence on the overall solution conductivity and compare it with a conductivity of 0.83% NaCl solution. The conductivity of the solution is very important in determining the corrosion rate/localization of the material and also affects the efficiency of the SVET measurements [74]. In this work, the conductivities of the MEM and 0.83% NaCl solution were comparable: 15 and 12 mS cm<sup>-1</sup>, respectively. Close conductivity values of two solutions indicate the reliability of the SVET results. Current densities were calculated taking into account these conductivities. Before SVET measurements the equipment was calibrated either in NaCl or in MEM electrolytes in accordance with [65]. Bulk pH of the solution during SVET/SIET measurements was constantly measured by means of a Sentron-SI pH-meter with MiniFET (#9202-010) pH-electrode. The drift of the potential was corrected on the basis of the bulk pH. The potential drift of the pH sensitive microelectrode is the result of change of the ionic equilibria (ion exchange) at the interfaces between the liquid membrane and inner/outer electrolyte [54,75–78].

The method of total anodic and cathodic current calculation from the SVET data [66,68], was used to simplify the presentation of a large amount of current density distribution maps. This method of data treatment firstly proposed by McMurray et al. [79,80] is applied by many scientific groups [66,68,81–84]. The evolution of the sum of total anodic and cathodic currents reveals the specimen activity during experiment. Therefore, this method can be applied to compare the electrochemical behaviour of different samples.

Using the integration of the current density ( $i_z$ ) distribution across the area of each SVET scan, the total anodic ( $I_{anodic}$ ) and cathodic ( $I_{cathodic}$ ) ionic current densities were calculated in accordance with following equations:

$$I_{anodic} = \int_{x_{min}}^{x_{max}} \int_{y_{min}}^{y_{max}} [i_z(x; y) > 0] dx dy, \quad (1)$$

$$I_{cathodic} = \int_{x_{min}}^{x_{max}} \int_{y_{min}}^{y_{max}} [i_z(x; y) < 0] dx dy, \quad (2)$$

where the  $x_{max}$ ,  $x_{min}$ ,  $y_{max}$  and  $y_{min}$  are the coordinates of the specimen scanned region. The total cathodic and anodic currents calculated from the investigated area will be presented in  $\mu A$  due to the integration of current density ( $\mu A \text{ cm}^{-2}$ ) and spatial dimensions of the scanned zone ( $\mu m$ ). In the current work, the evolution of the sum of total cathodic and anodic currents moduli as well as the separate total anodic and cathodic currents evolution during experiment for MA8 Mg alloy samples in MEM and 0.83 % NaCl solution were presented. To exclude the possible noise contribution to the integral current calculation we have also used  $5 \mu A \text{ cm}^{-2}$  as the minimal threshold value for integration (i.e. all values, which were in the range from  $-5 \mu A \text{ cm}^{-2}$  up to  $5 \mu A \text{ cm}^{-2}$  were excluded from the graph). The measurement error, in this case, did not exceed 5 %.

On the base of SVET maps, the evolution of anodic current density peak ( $i_{a,max}$ ) and cathodic current density peak ( $i_{c,max}$ ) were plotted to characterize the intensity of electrochemical processes in two media.

### **2.3. Immersion experiments and hydrogen evolution tests**

0.83 % NaCl solution and MEM with initial pH of 7.15 and 7.40, respectively, were used to expose the MA8 Mg alloy. For immersion and hydrogen evolution tests the lateral faces of rectangular samples were not isolated and were included in the total area of exposure. The bulk pH of the solution was measured daily. The experiment was performed at room temperature [85].

Immersion experiments were performed for a period of up to 30 days. Five samples of  $15 \times 20 \times 1.5 \text{ mm}^3$  were placed in 1000 mL of solution, which did not contact the air. Before the experiment, the surface of samples was prepared in the same way (according to the methodic in the 2.1. Section). The error in measuring the area did not exceed 3%. All the experiments were done in triplicates.

Hydrogen evolution tests were performed during 4, 7 and 30 days under different conditions. 7 and 30 days tests were performed using eudiometers (art. nr. 2591-10-500 from Neubert-Glas, Germany), which excludes the contact of the testing solution with  $\text{N}_2$ ,  $\text{O}_2$  and  $\text{CO}_2$  from the air. 3.575 g MA8 Mg alloy coupon was put in the solution container (500 mL) of eudiometer. We used five specimens with total surface area of about  $35 \text{ cm}^2$  (each of samples had a total area of about  $7 \text{ cm}^2$ ). The ratio of the sample surface area to solution volume was  $1:14 \text{ cm}^2 \text{ mL}^{-1}$ . In the experiment that lasted for 30 days, the MEM was not refreshed. For 7 days tests MEM was renewed every 12 h. These tests were done in two ways: with and without dry heat sterilizing the glass equipment in the drying chamber at  $180 \text{ }^\circ\text{C}$  during 1 h [86] before the experiment.

For 4 days tests MEM was used with flow-through cell. In this case, the dynamic hydrogen evolution was also employed to investigate the corrosion behaviour of MA8 in MEM. In this part, a common device (upturned burette combined with funnel and beaker) was used. The ratio of the sample surface area to solution volume was  $1:25 \text{ cm}^2 \text{ mL}^{-1}$ . During the measurement, a peristaltic pump was used to refresh the corrosive medium continuously with the speed of  $1.2 \pm 0.2 \text{ mL min}^{-1}$ . In this test, solutions were in contact with the air. The schematic of this experiment is shown in Fig. 2b (MEM was used as an example). 4 and 7 days tests were used to better imitate the medium refresh process in the human body and to prevent the depletion of the ionic components in the media.

Solutions in all tests were constantly stirred at  $350 \pm 100 \text{ rpm}$ . To confirm the results, hydrogen evolution tests were performed three times for each system. The measurement error did not exceed 10 %.

### **2.4. Corrosion product characterization**

At the end of the immersion experiments, the samples were removed from the solution, rinsed with deionized water and dried in air. X-ray diffraction (XRD) analysis was used to

characterize the phases of the corrosion products formed on the MA8 Mg alloy surface. XRD measurements of the specimens were performed using a D8 ADVANCE diffractometer (Bruker, Germany) in CuK $\alpha$  radiation, the tube power 40 kV, 40 mA at room temperature. The angle measurements were performed in the range  $2\theta = 5^\circ - 90^\circ$  with a step of  $0.02^\circ$ . The detailed characterization of the corrosion film formed on the MA8 Mg alloy surface in MEM was made using a SmartLab diffractometer (Rigaku, Japan) in CuK $\beta$  radiation, the tube power 42 kV, 140 mA at room temperature. The angle measurements were performed in the range  $2\theta = 9^\circ - 90^\circ$  with a step of  $0.01^\circ$ . All the experiments were done in triplicates.

The morphologies of the corrosion product formed on the MA8 Mg alloy surface in MEM and 0.83 % NaCl solutions, were examined by a scanning electron microscope (Zeiss EVO 40, Carl Zeiss Group, Germany). SEM-images of the film surface were obtained at an accelerating voltage of 20 kV. The microscope was equipped with Silicon Drift Detector X-Max<sup>N</sup> 80 (Oxford Instruments NanoAnalysis, USA). The distribution of elements in the corrosion product layer was obtained using an Energy Dispersive X-Ray (EDX) Analysis. The EDX measurements were controlled using AZtec 3.0 SP2 software (Oxford Instruments NanoAnalysis, USA). The nanoscale Cr layers were deposited on the sample surfaces to reduce image distortion associated with charging of the non-conductive layer. During the EDX data analysis, the chromium peaks were excluded.

### 3. Results

#### 3.1. Study of the localized corrosion process on the MA8 Mg alloy

Compared to 0.83 % NaCl solution, MEM contains a number of organic components (Table 2), which might adsorb on the Pt black deposited tip of the SVET probe or get extracted to the lipophilic phase of the liquid membrane cocktail of SIET probe. In both cases, the response of the probe would be altered. In order to study the influence of the MEM media on the capacitance of the SVET probe and on the Nernst slope of SIET H<sup>+</sup>-microelectrode as well as to establish the acceptability of the MEM media for SVET/SIET tests the following experiment was done. Every hour SVET/SIET experiments were carried out in the cell with MEM solution without the sample during 16 h. The results indicate the capacitance of the SVET probe as well as the Nernst slope for SIET microelectrode did not sufficiently change during the immersion and scanning in the MEM solution. The Nernst slope was  $56.0 \pm 0.7$  mV pH<sup>-1</sup>. SVET has detected the current density gradient in the solution from  $-4$  up to  $5$   $\mu\text{A cm}^{-2}$ . Thus, these results show the acceptability of the MEM media for SVET and SIET tests.

Fig. 3 depicts optical images of the investigated area (limited by frame) as well as SVET and SIET maps after 2, 24, 48 and 70 h exposure to 0.83 % NaCl solution. SVET and SIET have detected the formation of the cathodic zones (zone with higher values of the negative current density and with higher pH, blue area) immediately after sample immersion in NaCl solution (Fig. 3 1a, 1b, 1c). Higher values of the pH up to 10.8 are caused by the water reduction and dissolved oxygen reduction cathodic reactions (3, 4) [33,37,87].





For the *in vitro* corrosion test of biomedical Mg-based materials, the neutrality of the media is desirable. It is beneficial for mimicking the real body fluid environment. In practical, Mg dissolution can increase the bulk pH up to 10–11 of the non-buffered solutions [18,88], local pH has also been shown to reach values of above 10–11 [37,38,53], even in pH buffered electrolytes [25,51,54]. The pH of real body fluids is always stable since their good buffer capacity. However, the intensive formation of  $\text{OH}^-$  due to cathodic reactions (3,4) is detrimental for the life, since the alkaline pH can cause inflammation to the surrounding tissue [18].

With increase of the exposure time of the Mg alloy sample in the 0.83 % NaCl solution, cathodic areas become more localized and well correlated with optical images of the area under study (Fig. 3 2a, 3a, 4a). Anodic areas (zone with higher values of the positive current density and with lower values of the pH, red-orange area) were also registered by SVET and SIET.

Fig. 4 shows the optical images of the studied area (limited by frame) and SVET/SIET maps after 2, 24, 48 and 70 h of the material exposure to MEM. SVET diagrams demonstrate higher current density gradient from  $-60$  up to  $60 \mu\text{A cm}^{-2}$  than for the sample in 0.83 % NaCl medium (from  $-20$  up to  $20 \mu\text{A cm}^{-2}$ ) (Figs. 3 1b, 4 1b). Such high electrochemical activity is related to more complex composition of the MEM, presence of organic components and therefore, with the specific processes of the corrosion products formation [18]. Note that current density distribution for the sample exposed to MEM is more localized, compared to that for the samples exposed to NaCl solution. Moreover pitting like features characteristic for MEM exposure get passivated in time and new active spots activate (their location is different in all 4 maps, Fig. 4). In contrast to this, active spots developed at the beginning of immersion in NaCl solution, remain active throughout all immersion period (their location is constant in all 4 maps, Fig. 3), of up to 3 days (actually, part of the activity taking place in growing defects might have not been even detected by SVET). Similar effect was noticed in our previous work [54] where filiform corrosion was more characteristic for the sample where formation of hydroxyapatite-like corrosion products stabilized the local pH values at the value below 8.5. Presence of  $\text{Ca}^{2+}$  in MEM (Table 2) stimulated formation of hydroxyapatite-like compounds. This resulted in low local pH in Fig. 4 clearly indicating these products formation. Such hydroxyapatite-like compounds formed on the surface can serve as a partially protective film against corrosion of the material. The average pH for the sample in MEM did not exceed 8.0. Cathodic areas were also detected by SVET/SIET for the sample in MEM (Fig. 4). pH in these zones had the average value  $8.5 \pm 0.6$ . Cathodic and anodic areas registered by localized techniques were also well correlated with images obtained by optical microscopy (Fig. 4 2a, 3a, 4a). Fig. 4 4a, which depicts optical image of the investigated area after SVET/SIET studies, presents the sample without MEM solution for better revealing the bright cathodic zones. Red colour of MEM (Fig. 4 2a, 3a) is related to the presence of the phenol red in the MEM (Table 2). SVET and SIET maps (Figs. 3, 4) were plotted with the fixed values of current density scales and pH in each specific electrolyte to better show the changes of the respective

parameters over time. Exceptions are SIET maps in the Fig. 4, where wide range of the pH did not allowed to present all four diagrams in the same scale.

### 3.2. Corrosion performance of the MA8 Mg alloy

The evolution of the sum of total cathodic and anodic currents for the MA8 magnesium alloy sample in MEM and 0.83 % NaCl is presented in Fig. 5a. The total current data were used for an indication of the corrosion mechanism.

Different trends are registered for MA8 Mg alloy in two solutions. For the sample in MEM the period of high corrosion activity is observed from 5 up to 23 hours, values of the total current are intensively changed in the range from 0.5 up to 3.5  $\mu\text{A}$ . After 24 h, the total current decreases and reaches the minimum value at the end of the experiment (0.11  $\mu\text{A}$ , 70 h). It should be noted that total current behaviour has a wave-like trend with a period of increase, which is followed by a period of decrease. Such behaviour can be related to continuous process of corrosion film formation and destruction, with heterogeneous corrosion and passivation, which were studied by SVET/SIET (Fig. 4).

For the sample in 0.83% NaCl solution the trend of decrease the total currents is observed during all experimental time from 0.5  $\mu\text{A}$  (0 h) down to 0.13  $\mu\text{A}$  (70 h). Values of the current for the sample in MEM are higher than ones for the specimen in 0.83 % NaCl practically during all the experimental time and only after 60 h the values for the two systems become equal. These tendencies are averaged by trend presented in Fig. 5a as dotted lines.

The separate plots of total cathodic and anodic currents evolution are presented in Figs. 5b, 5c. Both total  $I_{\text{anodic}}$  and  $I_{\text{cathodic}}$  followed the same trend. Their discrepancy of the absolute value is due to the localized stirring of the solution and the duration of the SVET/SIET scanning time [68]. It should be noted that SVET is not always capable to detect all localized currents [66]. Therefore, the discrepancy between total  $I_{\text{anodic}}$  and  $I_{\text{cathodic}}$  are usually seen by SVET, since all current density values, which are presented on a SVET map, were not captured at the same time. It means that during one scan the corrosion behaviour of the sample and current distribution on the examined area can change [81]. The duration of one SVET/SIET scan was about 30 min.

Analysis of the evolution of anodic and cathodic current density peaks (Fig. 6) also shows the higher intensity of electrochemical processes in MEM as compared to 0.83 % NaCl solution. The graphs had similar trends, where  $i_{\text{a,max}}$  and  $i_{\text{c,max}}$  decreased over the time of the experiment, except for several peaks.

The evolution of local pH distribution for the MA8 Mg alloy in MEM and 0.83 % NaCl medium measured using SIET presents in Fig. 7 as the maximum and minimum pH values ( $\text{pH}_{\text{max}}$  and  $\text{pH}_{\text{min}}$ , respectively) (a) and the maximum pH difference ( $\Delta\text{pH}$ ) between pH values in anodic and cathodic areas versus time (b). As mentioned in the work [66] the  $\Delta\text{pH}$  provides an indication of the stability of the measured pH for the specimen under study.

For the sample in MEM the period of sample exposure can be characterized by the tendency of continuous  $\text{pH}_{\text{max}}$  and  $\text{pH}_{\text{min}}$  decrease down to 7.4 and 6.8, respectively (49 h). During the

experiment, average values of the  $\text{pH}_{\text{max}}$  and  $\text{pH}_{\text{min}}$  for the sample in MEM were  $8.5 \pm 0.6$  and  $7.5 \pm 0.4$ , respectively, with only random active areas reaching up to 9.8 (in Fig. 7a).

The specimen in 0.83 % NaCl demonstrates opposite tendency of the pH changing. Increase of the  $\text{pH}_{\text{max}}$  and  $\text{pH}_{\text{min}}$  was observed during the experiment (from 9.9 and 6.6 up to 10.8 and 8.8, respectively). The pH increasing tendency predominated during sample exposure to 0.83 % NaCl solution and supported by the polynomial trend line presented in the Fig. 7a. Average values of the  $\text{pH}_{\text{max}}$  and  $\text{pH}_{\text{min}}$  for the sample in 0.83 % NaCl were sufficiently higher than ones for MEM,  $10.5 \pm 0.2$  and  $8.0 \pm 0.4$ , respectively.

These results indicate that MEM due to its complex composition, presence and formation of organic and inorganic components in the solution and sample surface do not lead to the typical pH increase during the magnesium alloy corrosion, which is observed in 0.83 % NaCl solution (where water reduction reaction shifts pH to more alkaline range). These data are corroborated with bulk pH measurements in the MEM and 0.83 % NaCl solutions during 70 h of sample exposure (Fig. 7c). These bulk pH measurements were performed during SVET/SIET tests in order to correct the local pH in case of the drift of potential. Within the first 4 h of the sample immersion, the bulk pH of the 0.83 % NaCl solution achieved 10.4 and through the next hours it had a stable value of 10.8 until the end of the experiment. The bulk pH for the sample in MEM did not sufficiently change with time and had average value of about  $7.6 \pm 0.3$ .

Analyzing the  $\Delta\text{pH}$  evolution with time (shown in Fig. 7b), the sample in MEM demonstrates the small variations from 1.1 down to 0.7.  $\Delta\text{pH}$  for the sample in NaCl solution is higher than that for MEM and varies between 3.3 and 2.7, indicating the lower corrosion stability as compare to the sample in MEM.

These results indicate the different tendencies of the corrosion process passing on the surface of magnesium alloy in MEM and 0.83 % NaCl solution as well as the different tendencies of the corrosion products accumulation, which can reduce the activity of the material for the initial time of sample immersion.

### **3.3. Immersion experiments of MA8 Mg alloy samples and corrosion product analysis**

Fig. 8 depicts the results of the hydrogen evolution tests (a) coupled with daily measurements of the bulk pH (b) for MA8 magnesium alloy samples in MEM and 0.83 % NaCl solutions. These tests were performed using eudiometers during 30 days without solution refreshment. From the diagram of normalized hydrogen evolution rate, different tendencies can be revealed in two media. The hydrogen evolution for the specimens in 0.83 % NaCl occurs gradually without sharp increase and drop. Its average rate can be calculated for the all period of sample immersion as  $0.058 \pm 0.018 \text{ mL cm}^{-2} \text{ day}^{-1}$  ( $2.0 \pm 0.6 \text{ mL day}^{-1}$ ). More complicated situation is for the samples in MEM. One can determine four rates of hydrogen evolution. First one, (0 – 4 days) is  $0.031 \pm 0.019 \text{ mL cm}^{-2} \text{ day}^{-1}$  ( $1.1 \pm 0.7 \text{ mL day}^{-1}$ ). Second one, (5 day) is  $0.339 \text{ mL cm}^{-1} \text{ day}^{-2}$  ( $11.95 \text{ mL day}^{-1}$ ). Third one, (6 – 19 days) is  $0.015 \pm 0.009 \text{ mL cm}^{-2} \text{ day}^{-1}$  ( $0.5 \pm 0.3 \text{ mL day}^{-1}$ ). Fourth one, (20 – 30 days) is  $0.07 \pm 0.03 \text{ mL cm}^{-2} \text{ day}^{-1}$  ( $2.5 \pm 1.2 \text{ mL day}^{-1}$ ). From the analysis of these data it can be seen that hydrogen evolution rate for the

samples in MEM is predominately lesser than for the specimens in 0.83 % NaCl. The second and fourth rates are related to fluctuations that do not influence the general tendency. At the same time, the increase of hydrogen evolution during these periods was preceded by decrease of bulk pH, which can be seen from the diagram (Fig. 8b, curve for samples in MEM). pH decrease is related to presence of organic components in the MEM composition and with probable formation of organic acids (e.g. gluconic and lactic acids described in 4. Discussion) in the solution and on the surface of Mg alloy samples. It causes the partial destruction of the film of the corrosion products on the Mg alloy surface. After the film degradation the bare Mg alloy has a contact with medium again, which intensifies magnesium corrosion [33,37]. Therefore, intensification of the hydrogen evolution and pH increase are connected events and occurred at (3 – 6 days and 21 – 23 days). This trend of hydrogen evolution confirms the processes of formation and degradation of the surface film, which was detected using SVET (Figs. 4, 5). It should be noted, that corrosion of Mg alloy in MEM after the fourth day was going similar to the corrosion in NaCl solution due to MEM components depletion with time. Therefore, the final corrosion rate of samples in MEM seems comparable to that in 0.83 % NaCl solution. However, the differences in corrosion rate for Mg alloy in MEM and 0.83 % NaCl solution were reproducible. They are related to the different chemical composition of two media and to the processes of corrosive degradation of the sample. Bulk pH for the samples in 0.83 % NaCl increased for the first day up to 10.7 and stayed practically constant with the small variations  $10.7 \pm 0.1$ . These tendencies are averaged by polynomial trend presented in the Fig. 8b as dotted lines.

These data indicate that corrosion process as well as corrosion destruction of the MA8 magnesium sample in MEM occurs in rather complex way and obeys more complicated mechanism in comparison with typical Mg alloy corrosion in NaCl solution.

The results of 7 days hydrogen evolution tests are presented in Fig. 9. These tests were carried out in eudiometers in two ways: with and without dry heat sterilizing the glass equipment. MEM was refreshed every 12 h to exclude the acceleration of the magnesium corrosion due to formation of organic acids and to better imitate the influence of the human body media on the corrosion behaviour of the magnesium-based implant. Analysis of the data (Fig. 9) indicates the absence of the sharp increase of the hydrogen evolution, which was shown in the Fig. 8a. The average rate for the Mg alloy samples in unsterile conditions was  $0.025 \pm 0.008 \text{ mL cm}^{-2} \text{ day}^{-1}$  ( $0.9 \pm 0.3 \text{ mL day}^{-1}$ ) and  $0.017 \pm 0.009$  ( $0.6 \pm 0.3 \text{ mL day}^{-1}$ ) is sterilized setup. These rates were lower as compared to the ones determined for the 30 days immersed samples (without solution renewal). Due to the MEM refreshment every 12 h, the solution pH was stable without drops and sharp increase and had the average value of  $7.45 \pm 0.16$ . It should be noted that sterilization leads to the small hydrogen evolution rate decrease. Lower  $\text{H}_2$  rates in case of refreshed MEM solution can also be explained by the replenishment of ionic compounds (such as  $\text{Ca}^{2+}$ ,  $\text{HPO}_4^{2-}$  and  $\text{HCO}_3^-$ ) that get depleted due to formation of precipitate layer [25,26,54].

The data of the dynamic hydrogen evolution tests (combined with bulk pH monitoring) during 4 days of Mg alloy samples exposure to MEM using flow-through cell are shown in the Fig. 10. These tests were performed using upturned burette combined with funnel and beaker, the peristaltic pump was used to refresh the corrosive medium continuously. It should be noticed that experiment was stopped after about 100 h due to the continuous increase of the magnesium alloy corrosion after 32 h test, accompanied with sharp pH decrease of the MEM from 7.7 down to 6.5. The changes of corrosion rate and pH value are attributed to the contamination of MEM (due to microbial growth involving bacteria metabolism and probable formation of lactic and gluconic acids described in 4. Discussion). However, the lower corrosion rate of MA8 in MEM under dynamic condition at first 32 h measurement is correlated with data presented in the Fig. 9. Analysis of the hydrogen evolution rate indicates that this trend is close to the changes of cathodic and anodic total currents. The difference in time of the maximum of total anodic currents (7 h, Fig. 5) and the maximum volume of released hydrogen (after 32 h, Fig. 10) is due to the electrochemical reactions that do not contribute to the corrosive degradation of the material, as well as to the different ratio of the exposed material area to the volume of the aggressive medium. The issue of the surface to volume ratio has been discussed in the literature before [89,90] and is out of the scope of our paper. Despite different sample-surface-area-to-medium-volume ratios between SVET/SIET and hydrogen evolution tests, the comparative measurements in NaCl and MEM electrolytes were conducted at the same ratio. Figure 11 shows the XRD patterns of the MA8 Mg alloy after 30 days exposure to 0.83 % NaCl (a) and MEM (b, c). In the Fig. 11a, MgO and Mg(OH)<sub>2</sub> were identified in the corrosion products. Figure 11b depicts peaks responsible for MgO in the corrosion layer composition. The detailed XRD characterization of the corrosion film formed on MA8 Mg alloy in MEM (Fig. 11c) showed the presence of calcium magnesium phosphates (Ca<sub>2.89</sub>Mg<sub>0.11</sub>(PO<sub>4</sub>)<sub>2</sub>, Ca<sub>19</sub>Mg<sub>2</sub>(PO<sub>4</sub>)<sub>14</sub>). Figure 12 shows SEM morphology (a) and corresponding EDX spectra (b) of the corrosion product films formed on Mg alloy after immersion in 0.83 % NaCl solution (1a, 1b) and in MEM (2a, 2b; 3a, 3b) for 30 days. EDX analysis of the area 1 indicates the high concentration of Mg and O (23.7 and 62 at. %, respectively) in the film formed on the sample in NaCl solution and confirms the XRD data of the MgO and Mg(OH)<sub>2</sub> products formation. SEM images and EDX spectra recorded in the different areas of film (2, 3) formed on the material in MEM, shows other kind of surface with high content of Ca and P (2.4–9.5 and 1.1–5.8 at. %, respectively) based precipitation. Figure 13 depicts SEM morphology (a) of the film formed in MEM solution and corresponding EDX maps (b–f) of the element (C, Ca, P, Mg, O) distribution in this area. Analysis of these data reveals the two-layered structure of the film formed in MEM on MA8 Mg alloy, where outer layer consists of Ca and P precipitations, and the inner one includes Mg and O compounds. Formation of Ca – P – Mg – O precipitations can lead to the dynamic relocation of the anodic and cathodic zones along the surface, which were detected by SVET (Fig. 4).

#### 4. Discussion

Analysis of localized electrochemical measurement shows higher activity of the samples in MEM than in 0.83 % NaCl medium at the initial stage of exposure (Figs. 3, 4, 5, 6). This result can be interpreted by the specific process of biofilm formation. It should be distinguished in this article the terms of "electrochemical activity" and "corrosive degradation". The first one means the combination of electrochemical reactions taking place on the surface of investigated sample and high local current density recorded by SVET: anodic dissolution of metal substrate, hydrogen evolution as a result of electrochemical water reduction, dissolved oxygen reduction, formation and breakdown of surface layers (as a result of electrochemical and chemical reactions), adsorption and desorption related to electron transfer and distribution of electron density between various parts of the sample. At the same time, the term "corrosive degradation" means sample degradation as a result of chemical and electrochemical reactions occurred on its surface, which leads to the weight loss of the material. Thus, the term "electrochemical activity" involves the "corrosive degradation". Presence of organic components in the MEM leads to possible proliferation of the bacteria on the specimen surface that results in production of the lactic acid, which decrease the pH (Fig. 7a – local pH decreased down to 7.2–6.8 on the MA8 Mg alloy surface in MEM after 24–70 h). The pH evolution of MEM in the absence of Mg alloy is presented in Fig. 8c. The pH of the medium gradually decreased from 7.5 down to 6.5 due to the microbial growth and then slightly increased. Formation of hydroxyapatite-like corrosion products stabilized the local pH values at the value below 8.5. All these processes do not allow to increase the pH up to the values close to those typically observed during Mg corrosion in NaCl solution (Figs. 7a, 7c, 8b). Therefore, this high electrochemical activity is mainly related not to the corrosive degradation, but to the biofilm formation process. This hypothesis is based on the experimental results presented in Figure 5, which are difficult to interpret only by corrosive degradation of surface layers. Additionally, an increase in the current density recorded by SVET for magnesium alloy in MEM in comparison with values for the sample in NaCl solution can be related to bacterial metabolism and associated extracellular electron transfer, according to the work [91]. Moreover, SVET was originally designed for detecting the extracellular current near living cells [92]. This suggestion is confirmed by hydrogen evolution tests (Fig. 8a), which indicate that MA8 Mg alloy in MEM corroded at a lower rate than in 0.83 % NaCl during the entire immersion. It is related to the formation of partially protective layer of hydroxyapatite-like corrosion products (magnesium-substituted hydroxyapatite ( $\text{Ca}_a\text{Mg}_b(\text{PO}_4)_c(\text{OH})_d$ ) [54]) or  $\text{Ca}_{2.89}\text{Mg}_{0.11}(\text{PO}_4)_2$  and  $\text{Ca}_{19}\text{Mg}_2(\text{PO}_4)_{14}$  (Fig. 11c), which slows down  $\text{H}_2$  production. Hydroxyapatite-like compounds formed on Mg alloy in presence of  $\text{Ca}^{2+}$ ,  $\text{HPO}_4^{2-}$  and  $\text{HCO}_3^-$  are more protective than  $\text{Mg}(\text{OH})_2$  formed in NaCl solution. With some variations, our results are close to earlier reports [21,23,25,54,63,93,94], where main corrosion products found on Mg in solutions similar to MEM were hydroxyapatite, partially substituted with Mg ions and carbonate, and a mixture of different calcium phosphate (amorphous calcium phosphate (Ca/P: ~1.00) [23], tri-calcium phosphate (Ca/P: ~1.50) or octacalcium phosphate (Ca/P:~1.33)) [94].

During the corrosion process of MA8 Mg alloy, the generated  $\text{OH}^-$  are involved in the formation of hydroxyapatite-like compounds and therefore the formation of  $\text{Mg}(\text{OH})_2$  film is reduced following the complex chemical equilibrium at heterogeneous interface with electrolyte. XRD analysis of the corrosion products formed in MEM (Fig. 11b), where peaks responsible for  $\text{Mg}(\text{OH})_2$  are absent, confirms the aforementioned conclusion. It also should be noted that in accordance with the Pourbaix diagram for magnesium,  $\text{Mg}(\text{OH})_2$  is formed at pH values higher than 8.5 [21]. In NaCl electrolyte, the main precipitating compound is  $\text{Mg}(\text{OH})_2$ . Following the constant value of the solubility product, the local pH is then buffered at ca. 10.5 in presence of mM concentration of  $\text{Mg}^{2+}$ . The formation of  $\text{Mg}(\text{OH})_2$  film on the sample surface was detected by XRD (Fig. 11a). The local pH at Mg/MEM interface is lower because hydroxyapatite-like compounds precipitate at lower pH values (e.g. the pH of precipitation of stoichiometric hydroxyapatite is 7.0 at physiological concentration of the involved ions [25]). Formation of the hydroxyapatite-like compounds is governed by the constant values of their solubility products. Local pH is buffered by formed products as  $\text{OH}^-$  (generated by HER or ORR – reactions (3, 4)) are consumed for the formation of hydroxyapatite-like compounds, and do not increase the pH values.

It should be noted that acceleration of hydrogen evolution (Fig. 8a – test without MEM refreshing, Fig. 10 – test in flow-through cell) was not detected only for the system with 12 hours MEM renewal (Fig. 9). Due to the solution periodical renewal, the bacteria growth on the Mg alloy surface and in the MEM decreased. The possible formation of lactic acid that leads to the sharp pH decrease and Mg alloy corrosion increase was prevented. The results of this test indicate that corrosion is indirectly affected by bacterial metabolism due to pH changes. The replenishment of ionic compounds also contributes to the formation of corrosion film with higher protective properties as compared to the film without MEM refreshing, where depletion of ionic compounds, such as  $\text{Ca}^{2+}$ ,  $\text{HPO}_4^{2-}$  and  $\text{HCO}_3^-$  occurred. For the dynamic hydrogen evolution test performed in flow-through cell, although the media is refreshed in real time, the contamination of media is uncontrollable since the media directly contact with the air. This effect can to a certain extent be approximated to the SVET test, since the experiment condition were close to each other. Therefore, electrochemical activity detected by SVET in MEM and intensive hydrogen evolution can have the same origin. The effect of bacterial contamination of MEM under non-sterile conditions with the formation of lactic acid was established previously in [91,95]. As indicated in these works, the main reason (energy source) of the origin of microorganisms (bacteria, yeast, fungi, viruses, parasites, mycoplasma) is the presence of glucose in the MEM. This microbial growth is the reason for the pH indicator (phenol red) to be included in the composition of the commercial MEM. Therefore, in order to make the fair analysis of the samples degradation in MEM to imitate the real corrosion process in the human body, the experiment must be performed in sterile conditions, or the solution should be changed periodically to slow down bacteria growth [95,96]. Common streptomycin-penicilline can also be used to control the microbial growth.

Due to rather complex composition of the MEM, the activity of the magnesium alloy at the initial stage of the exposure, which was measured by SVET/SIET (Fig. 5), can be related to the film formation, as a result of corrosion product accumulation, which can include inorganic compounds (mainly containing calcium-phosphate and carbonate) [21,54].

MEM contains chloride ions, which typically accelerate corrosion, whereas  $\text{Ca}^{2+}$ , carbonate and phosphate present in this medium promote the formation of protective or partially protective layers.

The normal pH of MEM is 7.0–7.4; however, during the magnesium alloy exposure local variations of the pH can occur according to the SIET results. This makes the corrosion behaviour very complicated. For example, during the Mg alloy immersion in MEM the following processes may occur: the pH increase (Fig. 8b) can promote precipitation of Ca-phosphate on the material surface [63,97]; chloride ions attack the alloy surface with the destruction of  $\text{MgO/Mg(OH)}_2$  [18,98]; carbonates can also incorporate in the growing surface layers [4,19,21].

Amino acids in MEM influence magnesium (and other metals) corrosion by means of chelation reactions of metal cations. This point was also listed by Yamamoto et al. [19]. In [18] it is indicated that besides the different stability of the chelate complexes between  $\text{Mg}^{2+}$  and different amino acids, the isoelectric points also change. Consequently, diverse interactions between the charged Mg surface and positively or negatively charged amino acids could happen. The results of the work [19] showed that insoluble salt formation as well as protein adsorption delayed magnesium degradation, whereas organic compounds such as amino acids accelerated magnesium dissolution. Presence of sodium bicarbonate in MEM can also decrease the degradation rate of MA8 Mg alloy during the specimen exposure, since  $\text{HCO}_3^-$  participates in hydroxyapatite layer formation by supporting the favourable pH [54].

The reason of the pH changes (Figs. 7a, 7c, 8b) can be related not only to bacteria growth and formation of lactic acid, but also to the glucose presence in the solution. Effects of glucose on the corrosion behaviour of pure magnesium in saline and Hank's solutions were studied by Zeng et al. [98]. Significant difference in corrosion behaviour of pure magnesium was established in two types of media. Glucose intensifies corrosion of pure Mg in saline solution, while decelerates its corrosion in Hank's solution by means of the effect of such species as  $\text{Ca}^{2+}$  and phosphate ions. At the same time, authors in [98] worked with high glucose concentration 2.5% and 5%. In our work, MEM has 0.1% of glucose. In the previous work [99], it was shown that 0.05M glucose in solution has little influence on Mg corrosion in 0.5% NaCl electrolyte. The effect of glucose was also found to be alloy specific. Therefore, 0.0056 M glucose in MEM does not significantly influence the corrosion rate of MA8 alloy. Nevertheless, the electrochemical activity of the MA8 Mg alloy samples in MEM, which was measured on a microscale level by SVET/SIET, can be partly related to the following processes, discussed below.

Glucose ( $\text{CH}_2\text{OH(CHOH)}_4\text{CHO}$ ) can rapidly transform into gluconic acid ( $\text{CH}_2\text{OH(CHOH)}_4\text{COOH}$ ) in aqueous solutions. Mg gets attacked because of the pH decrease

and promotes adsorption of chloride ions on Mg surface and consequently accelerates corrosion [100]. Similarly to the aggressive  $\text{Cl}^-$  ions, gluconic acid formed in MEM, can also contribute to the formation of defects in the surface film (undermining  $\text{Mg}(\text{OH})_2$  – formed according to the reactions (3–6), and hydroxyapatite-like layers, which results in ruptures, and pits in the surface film), thus intensifying the corrosion process. Thereby, corrosion attacks from the  $\text{Cl}^-$  ions and gluconic acid enlarge voids on the surface film, which makes it easier for the solution to pass through the pores into the substrate and increase the Mg alloy dissolution activity. Such chloride-containing compounds as  $5\text{Mg}(\text{OH})_2 \cdot \text{MgCl}_2$ ,  $\text{MgCl}_2 \cdot 6\text{H}_2\text{O}$  or  $\text{Mg}_3(\text{OH})_5\text{Cl} \cdot 4\text{H}_2\text{O}$  can be included in the composition of the surface film during Mg alloy corrosion [101]. However, due to their low concentration, they were not detected in the XRD patterns (Fig. 11).



This indicates that presence of glucose in MEM might cause its acidity as the pH value decreases, according to the SIET data and bulk pH measurements (Figs. 7a, 7c, 8b). This acidification along with influence of lactic acid leads to the partial degradation of the corrosion products film and therefore, bare Mg alloy began to corrode again and after that the pH values rise gradually (reaction 3) with a new film formation. Thus, the dissolution and formation of a partially protective film formed on MA8 Mg alloy immersed in the glucose containing solution (MEM) result in a dynamic balance until the film becomes compact [54,98,102].

On the other hand, glucose was observed [98] to influence the corrosion layer formation on the Mg alloy by means of chelation reaction with  $\text{Ca}^{2+}$  ions according to (7):



Due to high solubility of calcium gluconate,  $\text{Ca}^{2+}$  ions can subsequently react with  $-\text{H}_2\text{PO}_4^-$  in MEM solution to form hydroxyapatite-like compounds and other calcium phosphate precipitates (i.e., octa-calcium phosphate, calcium dihydrogenphosphate monohydrate) [98].

To sum up, glucose in MEM can have two functions: it decreases the medium pH due to the transformation into gluconic acid and promotes the Ca-P layer formation due to the chelating reaction with  $\text{Ca}^{2+}$  ions [98].

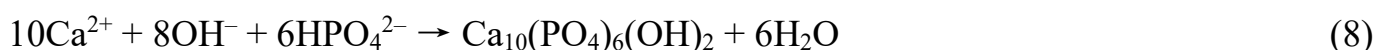
In [98] it was also established that increase of glucose concentration in Hank's solution promoted the formation of the Ca-P precipitates, and thus increase the corrosion resistance of pure Mg. At the same time, the results of the study [102] showed that low glucose concentration, i.e.  $1.0 \text{ g L}^{-1}$ , decreases the corrosion rate of magnesium alloy AZ31, whereas the presence of  $2.0$  or  $3.0 \text{ g L}^{-1}$  glucose increases the corrosion rate during long term immersion in saline solution. At low content, glucose due to complexing with  $\text{Mg}^{2+}$  ions can inhibit the influence of  $\text{Cl}^-$  ions, whereas at high concentrations it increases the degradation progress, which is related to the glucose transformation into gluconic acid and thus promoted  $\text{Cl}^-$  ions adsorption on the sample surface [102]. Therefore, the positive effect of glucose to improve Mg alloy corrosion resistance can be also applied to this work, since concentration of glucose

in MEM is also low (1 g L<sup>-1</sup>). However, its effect is significantly lower than the effect of Ca<sup>2+</sup>, HPO<sub>4</sub><sup>2-</sup> and HCO<sub>3</sub><sup>-</sup>.

Formation of the gluconic and lactic acids can increase the corrosion rate of the magnesium alloy samples. In particular, the increase in the volume of released hydrogen (Figs. 8, 10) and high values of integrated currents (Fig. 5) and current densities (Fig. 6) can be related to a film undermining by means of acids formed as a result of bacterial metabolism (lactic acid), and chemical reactions of the glucose transformation into gluconic acid. These acids formed in MEM offset OH<sup>-</sup> ions produced due to Mg corrosion and bind Mg<sup>2+</sup> and Ca<sup>2+</sup> cations. At the same time, high performance liquid chromatography detected neither gluconic nor lactic acids in the composition of the solution (at the end of 168 hours exposure tests) due to their low concentration. Nevertheless, the probability of the formation of these acids cannot be excluded taking into account the conditions implemented in this system [91,95,98,102].

In accordance with the EDX data (Fig. 13), the film formed during the specimen immersion in MEM solution has at least a two-layered structure. This point was also established by Wang et al. [63] who detected that corrosion products formed on the Mg-Zn-Ca alloy in DMEM consisted of two main layers, an inner layer composed of Mg and O and an outer layer composed mainly of Ca and P. Similarly, in SBF electrolyte, Mei et al. [25] could separate calcium-rich outer layer, from the inner layer of MgO/Mg(OH)<sub>2</sub> by EIS. The former manifests itself by fast growing new high frequency time-constant, whereas the latter was identified at the middle frequency part of EIS spectra. An inner MgO-Mg(OH)<sub>2</sub> layer (Figs. 13e, 13f) was formed as a result of traditional reaction of Mg<sup>2+</sup> ions released during corrosion with OH<sup>-</sup> from cathode sites [103,104]. Precipitation of calcium phosphate compounds (Ca-P) as an outer layer (Figs. 13c, 13d) has occurred due to the increase of local pH during the corrosion, as it noted in [97]. Formation of Ca-P layer was confirmed by XRD data, which indicate the presence of calcium magnesium phosphates in the composition of the corrosion film (Fig. 11c).

The results of the work [21] also showed formation of a double corrosion product layer on the magnesium alloy surface during the immersion in DMEM solution at room temperature consisting of an inner porous and an outer compact parts. Further surface analysis indicates that the formed layers mainly consist of calcium phosphates. Ca/P ratios show values around 1.67, indicating the formation of hydroxyapatite [21]. The work [98] also confirmed the precipitation probability of various types of Ca-phosphates from the body fluids. Therefore, the reaction (8) is possible:



The presented mechanism of Ca-P precipitation formation on the magnesium and Mg alloy surfaces can to a certain extent be applied to MA8 Mg alloy samples studied in MEM in the present work. According to the EDX analysis of the corrosion products, the high concentration of Ca and P was detected. The surface of this Ca-P-containing film has drought-like topography artefacts, due to the cracks that appeared as a result of layer degradation and

developing the corrosion process under the film (Figs. 12 2a, 12 3a, 13a). In accordance with this EDX spectrum data (Fig. 12 3b) the ratio of Ca/P is about 1.64, which is rather close to the hydroxyapatite products (1.67). Small deviations can be related to substitution of  $\text{Ca}^{2+}$  by  $\text{Mg}^{2+}$  and/or phosphate groups by carbonate groups [54,105,106]. The reaction (8) of hydroxyapatite formation permits the stabilization of the local pH during Mg alloy corrosion to lower values (below 9.0), which were registered by SIET. Presence of high amount of organic substances in MEM composition leads to the precipitation on the alloy surface products, which contain carbon (about 20 at. % of C). (Fig. 12 2b, 3b). However, carbon can hardly be quantified by EDX without dedicated calibration. Figure 13b indicates practically uniform distribution of carbon in both inner and outer layers of the film formed during sample immersion in MEM for 30 days. High content of C is also related to insoluble carbonate layer formation. Outer layer formed on the Mg alloy surface in MEM can be also divided in two parts: first one, with high content of Ca-P precipitation (Fig. 12 3b) and second one, with high amount of Mg (Fig. 12 2b). High Mg content (18.5 at. %) is mainly related to MgO formation, which was supported by XRD analysis (Fig. 11b). The SEM and SEM-EDX images of the film, formed in MEM (Figs. 12 and 13), indicate its complex morphology with various cracks on the surface, which is a result of dynamic process of the film formation and degradation due to accumulation and dissolution of the corrosion products.

All these facts show the necessity of studying the process of magnesium biodegradation not in typical NaCl medium but in solution of more complex composition, which represents the body fluid environments. It should be emphasized that MEM, which was used in this work, is appropriate for studying the electrochemical process on the magnesium alloy surface by SVET and SIET.

At the same time, such solutions as DMEM, MEM, HBSS or SBF are only partially representative for human body medium composition and from the chemical viewpoint, the composition of body fluids is much more complicated. In the human body various processes occur, i.e. proteins and cells can adhere to the magnesium alloy surface [107]; cells on the implant surface can produce lactic acid; proteins in medium can bind  $\text{Mg}^{2+}$  and  $\text{Ca}^{2+}$  cations, etc. The detailed role of the different amino acids, as well as other organic constituents of MEM, is still under exploration.

Due to the high electrochemical activity of the Mg alloy even in cell culture medium detected in this work, to control the biodegradation process of the material, samples must be protected by bioactive/bioinert coatings with further investigation of the corrosion activity. Moreover, the differentiation between corrosive degradation and electrochemical activity, which sometimes are not identical, should be clarified by means of electrochemical impedance spectroscopy, potentiodynamic polarization methods in conjunction with a cross-section images of corrosion products precipitation. These are the tasks of our future studies.

## 5. Conclusion

Analysis of the electrochemical behaviour of MA8 magnesium alloy in MEM and 0.83 wt. % NaCl solutions revealed the following conclusions:

- 1) SVET and local pH measurements can be performed in rather complex biological medium such as MEM. No change of the microelectrode response (that might have been expected due to the interaction of the membrane components with the organic compounds constituting MEM) was recorded in the MEM environment over the period of 16 hours. The Nernst slope for pH microelectrode in MEM was stable and reproducible ( $56.0 \pm 0.7$  mV pH<sup>-1</sup>).
- 2) SVET/SIET data indicate different trends of the corrosion process on the surface of magnesium alloy in MEM or 0.83 wt. % NaCl solutions. Higher electrochemical activity for the samples in MEM than in 0.83 wt. % NaCl solution at the initial stage of the material immersion can be related to the lactic acid formed as a result of microbial growth and bacteria metabolism in non-sterile conditions or gluconic acid in media. Hydrogen evolution rate is predominately higher for the samples in 0.83 wt. % NaCl solution in comparison with MEM. Formation of partially protective magnesium-substituted hydroxyapatite layer stabilizes the local pH of MEM below 9.0 and slows down magnesium corrosion.
- 3) EDX data reveal two-layer structure of the film formed in MEM on MA8 Mg alloy, where the outer and inner layers consist of Ca – P and Mg – O precipitations, respectively. XRD analysis of the sample after 30 days of immersion showed the presence of Ca-Mg phosphates in the composition of the corrosion products.
- 4) MEM renewal every 12 h leads to the reduction of corrosion rate of the Mg alloy due to the low rate of the bacteria growth on the Mg alloy surface and in the MEM, and replenishment of ionic compounds such as Ca<sup>2+</sup>, HPO<sub>4</sub><sup>2-</sup>, HCO<sub>3</sub><sup>-</sup> and Mg<sup>2+</sup> that stimulate growth of partially protective layer of hydroxyapatite-like products.
- 5) The necessity of studying the process of magnesium biodegradation in solutions with complex composition, which imitate the medium of the human environment, but not in trivial NaCl has been pointed out. To control the biodegradation process and to slow down the degradation rate, the magnesium samples need to be protected by bioactive/bioinert coatings with further investigation of the corrosion activity.

### **Data availability**

The raw/processed data required to reproduce these findings cannot be shared at this time as the data also forms part of an ongoing study.

### **Acknowledgements**

Electrochemical measurements, immersion tests and corrosion product characterization were supported by the Grant of Russian Science Foundation (project no. 19-73-00078). XRD results were collected under the government assignments from Ministry of Science and Higher

Education of the Russian Federation (project no. 0265-2019-0001). Di Mei thanks China Scholarship Council for the award of fellowship and funding (no. 201607040051).

## References

- [1] K.U. Kainer, Magnesium – Alloys and Technology, DGM, 2003. doi:10.1002/3527602046.
- [2] B. Mordike, T. Ebert, Magnesium: Properties — applications — potential, *Mater. Sci. Eng. A.* 302 (2001) 37–45. doi:10.1016/S0921-5093(00)01351-4.
- [3] F. Cao, G.-L. Song, A. Atrens, Corrosion and passivation of magnesium alloys, *Corros. Sci.* 111 (2016) 835–845. doi:10.1016/J.CORSCI.2016.05.041.
- [4] S. Virtanen, Biodegradable Mg and Mg alloys: Corrosion and biocompatibility, *Mater. Sci. Eng. B.* 176 (2011) 1600–1608. doi:10.1016/J.MSEB.2011.05.028.
- [5] B. Heublein, R. Rohde, V. Kaese, M. Niemeyer, W. Hartung, A. Haverich, Biocorrosion of magnesium alloys: a new principle in cardiovascular implant technology?, *Heart.* 89 (2003) 651–6. <http://www.ncbi.nlm.nih.gov/pubmed/12748224> (accessed January 11, 2018).
- [6] M. Peuster, P. Beerbaum, F.-W. Bach, H. Hauser, Are resorbable implants about to become a reality?, *Cardiol. Young.* 16 (2006) 107. doi:10.1017/S1047951106000011.
- [7] P. Erne, M. Schier, T.J. Resink, The Road to Bioabsorbable Stents: Reaching Clinical Reality?, *Cardiovasc. Intervent. Radiol.* 29 (2006) 11–16. doi:10.1007/s00270-004-0341-9.
- [8] P. Zartner, M. Buettner, H. Singer, M. Sigler, First biodegradable metal stent in a child with congenital heart disease: Evaluation of macro and histopathology, *Catheter. Cardiovasc. Interv.* 69 (2007) 443–446. doi:10.1002/ccd.20828.
- [9] R. Erbel, C. Di Mario, J. Bartunek, J. Bonnier, B. de Bruyne, F.R. Eberli, P. Erne, M. Haude, B. Heublein, M. Horrigan, C. Ilesley, D. Böse, J. Koolen, T.F. Lüscher, N. Weissman, R. Waksman, PROGRESS-AMS (Clinical Performance and Angiographic Results of Coronary Stenting with Absorbable Metal Stents) Investigators, Temporary scaffolding of coronary arteries with bioabsorbable magnesium stents: a prospective, non-randomised multicentre trial, *Lancet.* 369 (2007) 1869–1875. doi:10.1016/S0140-6736(07)60853-8.
- [10] F. Witte, V. Kaese, H. Haferkamp, E. Switzer, A. Meyer-Lindenberg, C.J. Wirth, H. Windhagen, In vivo corrosion of four magnesium alloys and the associated bone response, *Biomaterials.* 26 (2005) 3557–3563. doi:10.1016/J.BIOMATERIALS.2004.09.049.
- [11] M.P. Staiger, A.M. Pietak, J. Huadmai, G. Dias, Magnesium and its alloys as orthopedic biomaterials: A review, *Biomaterials.* 27 (2006) 1728–1734. doi:10.1016/J.BIOMATERIALS.2005.10.003.
- [12] F. Witte, H. Ulrich, M. Rudert, E. Willbold, Biodegradable magnesium scaffolds: Part 1: Appropriate inflammatory response, *J. Biomed. Mater. Res. Part A.* 81A (2007) 748–756. doi:10.1002/jbm.a.31170.
- [13] F. Witte, H. Ulrich, C. Palm, E. Willbold, Biodegradable magnesium scaffolds: Part II: Peri-implant bone remodeling, *J. Biomed. Mater. Res. Part A.* 81A (2007) 757–765. doi:10.1002/jbm.a.31293.
- [14] F. Witte, J. Reifenrath, P.P. Müller, H.-A. Crostack, J. Nellesen, F.W. Bach, D. Bormann, M. Rudert, Cartilage repair on magnesium scaffolds used as a subchondral bone replacement, *Materwiss. Werksttech.* 37 (2006) 504–508. doi:10.1002/mawe.200600027.
- [15] D. Williams, New interests in magnesium., *Med. Device Technol.* 17 (2006) 9–10. <http://www.ncbi.nlm.nih.gov/pubmed/16736656> (accessed January 11, 2018).
- [16] B. a Shaw, E. Sikora, S. Virtanen, Fix, Heal, and Disappear: A New Approach to Using Metals in the Human Body, *Interface.* 17 (2008) 45–49. [https://www.electrochem.org/dl/interface/sum/sum08/su08\\_p45-49.pdf](https://www.electrochem.org/dl/interface/sum/sum08/su08_p45-49.pdf) (accessed January 11, 2018).
- [17] F. Witte, N. Hort, C. Vogt, S. Cohen, K.U. Kainer, R. Willumeit, F. Feyerabend, Degradable biomaterials based on magnesium corrosion, *Curr. Opin. Solid State Mater. Sci.* 12 (2008) 63–72. doi:10.1016/J.COSSMS.2009.04.001.
- [18] M. Esmaily, J.E. Svensson, S. Fajardo, N. Birbilis, G.S. Frankel, S. Virtanen, R. Arrabal, S. Thomas, L.G. Johansson, Fundamentals and advances in magnesium alloy corrosion, *Prog. Mater. Sci.* 89 (2017) 92–193. doi:10.1016/J.PMATSCI.2017.04.011.
- [19] A. Yamamoto, S. Hiromoto, Effect of inorganic salts, amino acids and proteins on the degradation of pure magnesium in vitro, *Mater. Sci. Eng. C.* 29 (2009) 1559–1568. doi:10.1016/j.msec.2008.12.015.
- [20] M.J. Coelho, A. Trigo Cabral, M.H. Fernandes, Human bone cell cultures in biocompatibility testing. Part I: Osteoblastic differentiation of serially passaged human bone marrow cells cultured in  $\alpha$ -MEM and in DMEM, *Biomaterials.* 21 (2000) 1087–1094. doi:10.1016/S0142-9612(99)00284-7.
- [21] V. Wagener, S. Virtanen, Protective layer formation on magnesium in cell culture medium, *Mater. Sci. Eng. C.* 63 (2016) 341–351. doi:10.1016/j.msec.2016.03.003.

- [22] H. Yang, K. Xia, T. Wang, J. Niu, Y. Song, Z. Xiong, K. Zheng, S. Wei, W. Lu, Growth, in vitro biodegradation and cytocompatibility properties of nano-hydroxyapatite coatings on biodegradable magnesium alloys, *J. Alloys Compd.* 672 (2016) 366–373. doi:10.1016/j.jallcom.2016.02.156.
- [23] R. Rettig, S. Virtanen, Composition of corrosion layers on a magnesium rare-earth alloy in simulated body fluids, *J. Biomed. Mater. Res. Part A.* 88A (2009) 359–369. doi:10.1002/jbm.a.31887.
- [24] Y. Wang, C.S. Lim, C.V. Lim, M.S. Yong, E.K. Teo, L.N. Moh, In vitro degradation behavior of M1A magnesium alloy in protein-containing simulated body fluid, *Mater. Sci. Eng. C.* 31 (2011) 579–587. doi:10.1016/j.msec.2010.11.017.
- [25] D. Mei, S. V. Lamaka, J. Gonzalez, F. Feyerabend, R. Willumeit-Römer, M.L. Zheludkevich, The role of individual components of simulated body fluid on the corrosion behavior of commercially pure Mg, *Corros. Sci.* 147 (2019) 81–93. doi:10.1016/j.corsci.2018.11.011.
- [26] D. Mei, S. V. Lamaka, C. Feiler, M.L. Zheludkevich, The effect of small-molecule bio-relevant organic components at low concentration on the corrosion of commercially pure Mg and Mg-0.8Ca alloy: An overall perspective, *Corros. Sci.* 153 (2019) 258–271. doi:10.1016/J.CORSCI.2019.03.039.
- [27] P.K. Bowen, J. Drelich, J. Goldman, Magnesium in the murine artery: Probing the products of corrosion, *Acta Biomater.* 10 (2014) 1475–1483. doi:10.1016/J.ACTBIO.2013.11.021.
- [28] S. Keim, J.G. Brunner, B. Fabry, S. Virtanen, Control of magnesium corrosion and biocompatibility with biomimetic coatings, *J. Biomed. Mater. Res. Part B Appl. Biomater.* 96B (2011) 84–90. doi:10.1002/jbm.b.31742.
- [29] X.N. Gu, Y.F. Zheng, L.J. Chen, Influence of artificial biological fluid composition on the biocorrosion of potential orthopedic Mg–Ca, AZ31, AZ91 alloys, *Biomed. Mater.* 4 (2009) 65011. doi:10.1088/1748-6041/4/6/065011.
- [30] Y. Xin, K. Huo, H. Tao, G. Tang, P.K. Chu, Influence of aggressive ions on the degradation behavior of biomedical magnesium alloy in physiological environment, *Acta Biomater.* 4 (2008) 2008–2015. doi:10.1016/J.ACTBIO.2008.05.014.
- [31] G. Williams, H.A.-L. Dafydd, H.N. McMurray, N. Birbilis, The influence of arsenic alloying on the localised corrosion behaviour of magnesium, *Electrochim. Acta.* 219 (2016) 401–411. doi:10.1016/J.ELECTACTA.2016.10.006.
- [32] S.V. Lamaka, O.V. Karavai, A.C. Bastos, M.L. Zheludkevich, M.G.S. Ferreira, Monitoring local spatial distribution of Mg<sup>2+</sup>, pH and ionic currents, *Electrochem. Commun.* 10 (2008) 259–262. doi:10.1016/J.ELECOM.2007.12.003.
- [33] A.S. Gnedenkov, S.L. Sinebryukhov, D.V. Mashtalyar, S.V. Gnedenkov, Localized corrosion of the Mg alloys with inhibitor-containing coatings: SVET and SIET studies, *Corros. Sci.* 102 (2016) 269–278. doi:10.1016/j.corsci.2015.10.015.
- [34] A.S. Gnedenkov, S.L. Sinebryukhov, D.V. Mashtalyar, S.V. Gnedenkov, Features of the corrosion processes development at the magnesium alloys surface, *Surf. Coatings Technol.* 225 (2013) 112–118. doi:10.1016/j.surfcoat.2013.03.023.
- [35] G. Williams, H.N. McMurray, R. Grace, Inhibition of magnesium localised corrosion in chloride containing electrolyte, *Electrochim. Acta.* 55 (2010) 7824–7833. doi:10.1016/j.electacta.2010.03.023.
- [36] N.T. Kirkland, G. Williams, N. Birbilis, Observations of the galvanostatic dissolution of pure magnesium, *Corros. Sci.* 65 (2012) 5–9. doi:10.1016/j.corsci.2012.08.029.
- [37] O.V. Karavai, A.C. Bastos, M.L. Zheludkevich, M.G. Taryba, S.V. Lamaka, M.G.S. Ferreira, Localized electrochemical study of corrosion inhibition in microdefects on coated AZ31 magnesium alloy, *Electrochim. Acta.* 55 (2010) 5401–5406. doi:10.1016/j.electacta.2010.04.064.
- [38] S.V. Lamaka, G. Knörnschild, D.V. Snihirova, M.G. Taryba, M.L. Zheludkevich, M.G.S. Ferreira, Complex anticorrosion coating for ZK30 magnesium alloy, *Electrochim. Acta.* 55 (2009) 131–141. doi:10.1016/j.electacta.2009.08.018.
- [39] W. Liu, F. Cao, Y. Xia, L. Chang, J. Zhang, Localized Corrosion of Magnesium Alloys in NaCl Solutions Explored by Scanning Electrochemical Microscopy in Feedback Mode, *Electrochim. Acta.* 132 (2014) 377–388. doi:10.1016/j.electacta.2014.04.044.
- [40] P. Dauphin-Ducharme, J. Mauzeroll, Surface Analytical Methods Applied to Magnesium Corrosion, *Anal. Chem.* 87 (2015) 7499–7509. doi:10.1021/ac504576g.
- [41] D. Snihirova, M. Taryba, S. V. Lamaka, M.F. Montemor, Corrosion inhibition synergies on a model Al-Cu-Mg sample studied by localized scanning electrochemical techniques, *Corros. Sci.* 112 (2016) 408–417. doi:10.1016/j.corsci.2016.08.008.

- [42] G. Williams, N. Birbilis, H.N. McMurray, The source of hydrogen evolved from a magnesium anode, *Electrochem. Commun.* 36 (2013) 1–5. doi:10.1016/J.ELECOM.2013.08.023.
- [43] X. Zheng, Q. Liu, H. Ma, S. Das, Y. Gu, L. Zhang, Probing local corrosion performance of sol-gel/MAO composite coating on Mg alloy, *Surf. Coatings Technol.* 347 (2018) 286–296. doi:10.1016/J.SURFCOAT.2018.05.010.
- [44] M.F. Montemor, A.M. Simões, M.J. Carmezim, Characterization of rare-earth conversion films formed on the AZ31 magnesium alloy and its relation with corrosion protection, *Appl. Surf. Sci.* 253 (2007) 6922–6931. doi:10.1016/J.APSUSC.2007.02.019.
- [45] A.S. Gnedenkov, S.L. Sinebryukhov, D. V. Mashtalyar, S. V. Gnedenkov, Microscale morphology and properties of the PEO-coating surface, in: *Phys. Procedia*, 2012: pp. 98–101. doi:10.1016/j.phpro.2012.01.025.
- [46] A.S. Gnedenkov, S.L. Sinebryukhov, D.V. Mashtalyar, S.V. Gnedenkov, Features of the magnesium alloys corrosion in the chloride-containing media, *Solid State Phenom.* 213 (2014) 143–148. doi:10.4028/www.scientific.net/SSP.213.143.
- [47] S.V. Gnedenkov, S.L. Sinebryukhov, V.S. Egorkin, D.V. Mashtalyar, I.E. Vyaliy, K.V. Nadaraia, I.M. Imshinetskiy, A.I. Nikitin, E.P. Subbotin, A.S. Gnedenkov, Magnesium fabricated using additive technology: Specificity of corrosion and protection, *J. Alloys Compd.* 808 (2019) 151629. doi:10.1016/j.jallcom.2019.07.341.
- [48] L.C. Córdoba, A. Marques, M. Taryba, T. Coradin, F. Montemor, Hybrid coatings with collagen and chitosan for improved bioactivity of Mg alloys, *Surf. Coatings Technol.* 341 (2018) 103–113. doi:10.1016/J.SURFCOAT.2017.08.062.
- [49] D.K. Ivanou, K.A. Yasakau, S. Kallip, A.D. Lisenkov, M. Starykevich, S. V. Lamaka, M.G.S. Ferreira, M.L. Zheludkevich, Active corrosion protection coating for a ZE41 magnesium alloy created by combining PEO and sol-gel techniques, *RSC Adv.* 6 (2016) 12553–12560. doi:10.1039/C5RA22639B.
- [50] J. Izquierdo, L. Nagy, I. Bitter, R.M. Souto, G. Nagy, Potentiometric scanning electrochemical microscopy for the local characterization of the electrochemical behaviour of magnesium-based materials, *Electrochim. Acta.* 87 (2013) 283–293. doi:10.1016/J.ELECTACTA.2012.09.029.
- [51] S.S. Jamali, S.E. Moulton, D.E. Tallman, M. Forsyth, J. Weber, G.G. Wallace, Applications of scanning electrochemical microscopy (SECM) for local characterization of AZ31 surface during corrosion in a buffered media, *Corros. Sci.* 86 (2014) 93–100. doi:10.1016/J.CORSCI.2014.04.035.
- [52] D. Mareci, G. Bolat, J. Izquierdo, C. Crimu, C. Munteanu, I. Antoniac, R.M. Souto, Electrochemical characteristics of bioresorbable binary MgCa alloys in Ringer's solution: Revealing the impact of local pH distributions during in-vitro dissolution, *Mater. Sci. Eng. C.* 60 (2016) 402–410. doi:10.1016/J.MSEC.2015.11.069.
- [53] U.M. Tefashe, P. Dauphin-Ducharme, M. Danaie, Z.P. Cano, J.R. Kish, G.A. Botton, J. Mauzeroll, Localized Corrosion Behavior of AZ31B Magnesium Alloy with an Electrodeposited Poly(3,4-Ethylenedioxythiophene) Coating, *J. Electrochem. Soc.* 162 (2015) C536–C544. doi:10.1149/2.0601510jes.
- [54] S. V. Lamaka, J. Gonzalez, D. Mei, F. Feyerabend, R. Willumeit-Römer, M.L. Zheludkevich, Local pH and Its Evolution Near Mg Alloy Surfaces Exposed to Simulated Body Fluids, *Adv. Mater. Interfaces.* 5 (2018) 1800169. doi:10.1002/admi.201800169.
- [55] S.V. Gnedenkov, S.L. Sinebryukhov, D.V. Mashtalyar, V.S. Egorkin, M.V. Sidorova, A.S. Gnedenkov, Composite polymer-containing protective coatings on magnesium alloy MA8, *Corros. Sci.* 85 (2014) 52–59. doi:10.1016/j.corsci.2014.03.035.
- [56] S.V. Gnedenkov, S.L. Sinebryukhov, D.V. Mashtalyar, K.V. Nadaraia, A.S. Gnedenkov, V.M. Bouznic, Composite fluoropolymer coatings on the MA8 magnesium alloy surface, *Corros. Sci.* 111 (2016) 175–185. doi:10.1016/j.corsci.2016.04.052.
- [57] A.S. Gnedenkov, S.L. Sinebryukhov, D.V. Mashtalyar, S.V. Gnedenkov, Protective properties of inhibitor-containing composite coatings on a Mg alloy, *Corros. Sci.* 102 (2016) 348–354. doi:10.1016/j.corsci.2015.10.026.
- [58] S.V. Gnedenkov, S.L. Sinebryukhov, D.V. Mashtalyar, I.M. Imshinetskiy, A.S. Gnedenkov, A.V. Samokhin, Y.V. Tsvetkov, Protective composite coatings obtained by plasma electrolytic oxidation on magnesium alloy MA8, *Vacuum.* 120 (2015) 107–114. doi:10.1016/j.vacuum.2015.02.004.
- [59] S.L. Sinebryukhov, A.S. Gnedenkov, D.V. Mashtalyar, S.V. Gnedenkov, PEO-coating/substrate

- interface investigation by localised electrochemical impedance spectroscopy, *Surf. Coatings Technol.* 205 (2010) 1697–1701. doi:10.1016/j.surfcoat.2010.05.048.
- [60] A.S. Gnedenkoy, S.L. Sinebryukhov, D. V. Mashtalyar, S. V. Gnedenkoy, Inhibitor-Containing Composite Coatings on Mg Alloys: Corrosion Mechanism and Self-Healing Protection, *Solid State Phenom.* 245 (2016) 89–96. doi:10.4028/www.scientific.net/SSP.245.89.
- [61] D.V. Mashtalyar, S.V. Gnedenkoy, S.L. Sinebryukhov, I.M. Imshinetskiy, A.S. Gnedenkoy, V.M. Bouzunik, Composite coatings formed using plasma electrolytic oxidation and fluoroparaffin materials, *J. Alloys Compd.* 767 (2018) 353–360. doi:10.1016/j.jallcom.2018.07.085.
- [62] K. Watchrarat, W. Korchunjit, S. Buranasinsup, J. Taylor, P. Ritruethai, T. Wongtawan, MEM &alpha; Promotes Cell Proliferation and Expression of Bone Marrow Derived Equine Mesenchymal Stem Cell Gene Markers but Depresses Differentiation Gene Markers, *J. Equine Vet. Sci.* 50 (2017) 8–14. doi:10.1016/j.jevs.2016.10.017.
- [63] J. Wang, Y. Jang, G. Wan, V. Giridharan, G.-L. Song, Z. Xu, Y. Koo, P. Qi, J. Sankar, N. Huang, Y. Yun, Flow-induced corrosion of absorbable magnesium alloy: In-situ and real-time electrochemical study, *Corros. Sci.* 104 (2016) 277–289. doi:10.1016/J.CORSCI.2015.12.020.
- [64] Thermo Fisher Scientific, Inc. US. <https://www.thermofisher.com/order/catalog/product/61100103#/61100103> (accessed January 17, 2020).
- [65] APPLICABLE ELECTRONICS SCANNING VIBRATING ELECTRODE TECHNIQUE (SVET) For Electrophysiology SYSTEM MANUAL, [www.applicableelectronics.com](http://www.applicableelectronics.com) (accessed January 17, 2020).
- [66] A. Alvarez-Pampliega, S.V. Lamaka, M.G. Taryba, M. Madani, J. De Strycker, E. Tourwé, M.G.S. Ferreira, H. Terryn, Cut-edge corrosion study on painted aluminum rich metallic coated steel by scanning vibrating electrode and micro-potentiometric techniques, *Electrochim. Acta.* 61 (2012) 107–117. doi:10.1016/j.electacta.2011.11.110.
- [67] A.C. Bouali, A.C. Bastos, S. V. Lamaka, M. Serdechnova, M.G.S. Ferreira, M.L. Zheludkevich, Evaporation of Electrolyte during SVET Measurements: The Scale of the Problem and the Solutions, *Electroanalysis.* 31 (2019) 2290–2298. doi:10.1002/elan.201900435.
- [68] M.F. Montemor, D.V. Snihirova, M.G. Taryba, S.V. Lamaka, I.A. Kartsonakis, A.C. Balaskas, G.C. Kordas, J. Tedim, A. Kuznetsova, M.L. Zheludkevich, M.G.S. Ferreira, Evaluation of self-healing ability in protective coatings modified with combinations of layered double hydroxides and cerium molybdate nanocontainers filled with corrosion inhibitors, *Electrochim. Acta.* 60 (2012) 31–40. doi:10.1016/j.electacta.2011.10.078.
- [69] V.A. Nazarov, M.G. Taryba, E.A. Zdrachek, K.A. Andronchyk, V. V. Egorov, S. V. Lamaka, Sodium- and chloride-selective microelectrodes optimized for corrosion studies, *J. Electroanal. Chem.* 706 (2013) 13–24. doi:10.1016/j.jelechem.2013.07.034.
- [70] M.G. Taryba, S. V. Lamaka, Plasticizer-free solid-contact pH-selective microelectrode for visualization of local corrosion, *J. Electroanal. Chem.* 725 (2014) 32–38. doi:10.1016/j.jelechem.2014.04.016.
- [71] R.S. Lillard, Scanning electrode techniques for investigating near-surface solution current densities, in: P. Marcus, F. Mansfeld (Eds.), *Anal. Methods Corros. Sci. Eng.*, CRC Press, Boca Raton, 2006.
- [72] O. Dolgikh, A. Demeter, S. V. Lamaka, M. Taryba, A.C. Bastos, M.C. Quevedo, J. Deconinck, Simulation of the role of vibration on Scanning Vibrating Electrode Technique measurements close to a disc in plane, *Electrochim. Acta.* 203 (2016) 379–387. doi:10.1016/j.electacta.2016.01.188.
- [73] S.V. Lamaka, M. Taryba, M.F. Montemor, H.S. Isaacs, M.G.S. Ferreira, Quasi-simultaneous measurements of ionic currents by vibrating probe and pH distribution by ion-selective microelectrode, *Electrochem. Commun.* 13 (2011) 20–23. doi:10.1016/j.elecom.2010.11.002.
- [74] A.C. Bastos, M.C. Quevedo, M.G.S. Ferreira, Preliminary research on the use of SVET in non-aqueous media, *Electrochim. Acta.* 202 (2016) 310–315. doi:10.1016/j.electacta.2015.12.107.
- [75] D. Ammann, *Ion-selective microelectrodes : principles, design, and application*, Springer-Verlag, 1986.
- [76] T.A.D. Patko, *Understanding Ion Selective Sensors*, 2009. <http://www.astisensor.com> (accessed February 3, 2020).
- [77] K.N. Mikhelson, *Ion-selective electrodes*, Springer, 2013.
- [78] A.K. Covington, *Ion-selective electrode methodology. Volume I*, CRC Press, 2018.

- [79] H.N. McMurray, D. Williams, D.A. Worsley, Artifacts Induced by Large-Amplitude Probe Vibrations in Localized Corrosion Measured by SVET, *J. Electrochem. Soc.* 150 (2003) B567. doi:10.1149/1.1623494.
- [80] D.A. Worsley, H.N. McMurray, J.H. Sullivan, I.P. Williams, Quantitative Assessment of Localized Corrosion Occurring on Galvanized Steel Samples Using the Scanning Vibrating Electrode Technique, *CORROSION*. 60 (2004) 437–447. doi:10.5006/1.3299239.
- [81] M. Yan, V.J. Gelling, B.R. Hinderliter, D. Battocchi, D.E. Tallman, G.P. Bierwagen, SVET method for characterizing anti-corrosion performance of metal-rich coatings, *Corros. Sci.* 52 (2010) 2636–2642. doi:10.1016/j.corsci.2010.04.012.
- [82] R.M. Souto, Y. González-García, A.C. Bastos, A.M. Simões, Investigating corrosion processes in the micrometric range: A SVET study of the galvanic corrosion of zinc coupled with iron, *Corros. Sci.* 49 (2007) 4568–4580. doi:10.1016/j.corsci.2007.04.016.
- [83] A. Gnedenkov, S. Sinebryukhov, D. Mashtalyar, I. Vyaliy, V. Egorkin, S. Gnedenkov, Corrosion of the Welded Aluminium Alloy in 0.5 M NaCl Solution. Part 1: Specificity of Development, *Materials (Basel)*. 11 (2018) 2053. doi:10.3390/ma11102053.
- [84] A.S. Gnedenkov, S.L. Sinebryukhov, D. V. Mashtalyar, I.E. Vyaliy, V.S. Egorkin, S. V. Gnedenkov, Corrosion of the welded aluminium alloy in 0.5 M NaCl solution. Part 2: Coating protection, *Materials (Basel)*. 11 (2018) 2177. doi:10.3390/ma11112177.
- [85] V. Wagener, S. Virtanen, Influence of Electrolyte Composition (Simulated Body Fluid vs. Dulbecco's Modified Eagle's Medium), Temperature, and Solution Flow on the Biocorrosion Behavior of Commercially Pure Mg, *CORROSION*. 73 (2017) 1413–1422. doi:10.5006/2510.
- [86] J.G. Solon, S. Killeen, Decontamination and sterilization, *Surg.* 37 (2019) 51–57. doi:10.1016/J.MPSUR.2018.11.002.
- [87] E.L. Silva, S. V. Lamaka, D. Mei, M.L. Zheludkevich, The Reduction of Dissolved Oxygen During Magnesium Corrosion, *ChemistryOpen*. 7 (2018) 664–668. doi:10.1002/open.201800076.
- [88] Z. Shi, M. Liu, A. Atrens, Measurement of the corrosion rate of magnesium alloys using Tafel extrapolation, *Corros. Sci.* 52 (2010) 579–588. doi:10.1016/J.CORSCI.2009.10.016.
- [89] N.T. Kirkland, N. Birbilis, M.P. Staiger, Assessing the corrosion of biodegradable magnesium implants: A critical review of current methodologies and their limitations, *Acta Biomater.* 8 (2012) 925–936. doi:10.1016/j.actbio.2011.11.014.
- [90] J. Gonzalez, R.Q. Hou, E.P.S. Nidadavolu, R. Willumeit-Römer, F. Feyerabend, Magnesium degradation under physiological conditions – Best practice, *Bioact. Mater.* 3 (2018) 174–185. doi:10.1016/j.bioactmat.2018.01.003.
- [91] S.I. Yamazaki, T. Kaneko, N. Taketomo, K. Kano, T. Ikeda, Glucose Metabolism of Lactic Acid Bacteria Changed by Quinone-mediated Extracellular Electron Transfer, *Biosci. Biotechnol. Biochem.* 66 (2002) 2100–2106. doi:10.1271/bbb.66.2100.
- [92] L.F. Jaffe, R. Nuccitelli, An ultrasensitive vibrating probe for measuring steady extracellular currents, *J. Cell Biol.* 63 (1974) 614–628. doi:10.1083/jcb.63.2.614.
- [93] P.K. Bowen, C.T. McNamara, O.P. Mills, J. Drelich, J. Goldman, FIB-TEM Study of Magnesium Corrosion Products after 14 Days in the Murine Artery, *ACS Biomater. Sci. Eng.* 1 (2015) 919–926. doi:10.1021/acsbiomaterials.5b00044.
- [94] O. Suzuki, Octacalcium phosphate: Osteoconductivity and crystal chemistry, *Acta Biomater.* 6 (2010) 3379–3387. doi:10.1016/J.ACTBIO.2010.04.002.
- [95] I. Marco, F. Feyerabend, R. Willumeit-Römer, O. Van der Biest, Degradation testing of Mg alloys in Dulbecco's modified eagle medium: Influence of medium sterilization, *Mater. Sci. Eng. C*. 62 (2016) 68–78. doi:10.1016/J.MSEC.2016.01.039.
- [96] S. Johnston, Z. Shi, C. Hoe, P.J. Uggowitzer, M. Cihova, J.F. Löffler, M.S. Dargusch, A. Atrens, The influence of two common sterilization techniques on the corrosion of Mg and its alloys for biomedical applications, *J. Biomed. Mater. Res. Part B Appl. Biomater.* 106 (2018) 1907–1917. doi:10.1002/jbm.b.34004.
- [97] R. Willumeit, J. Fischer, F. Feyerabend, N. Hort, U. Bismayer, S. Heidrich, B. Mihailova, Chemical surface alteration of biodegradable magnesium exposed to corrosion media, *Acta Biomater.* 7 (2011) 2704–2715. doi:10.1016/J.ACTBIO.2011.03.004.
- [98] R.-C. Zeng, X.-T. Li, S.-Q. Li, F. Zhang, E.-H. Han, In vitro degradation of pure Mg in response to glucose, *Sci. Rep.* 5 (2015) 13026. doi:10.1038/srep13026.

- [99] S.V. Lamaka, B. Vaghefinazari, D. Mei, R.P. Petrauskas, D. Höche, M.L. Zheludkevich, Comprehensive screening of Mg corrosion inhibitors, *Corros. Sci.* 128 (2017) 224–240. doi:10.1016/J.CORSCI.2017.07.011.
- [100] L.-Y. Cui, X.-T. Li, R.-C. Zeng, S.-Q. Li, E.-H. Han, L. Song, In vitro corrosion of Mg–Ca alloy — The influence of glucose content, *Front. Mater. Sci.* 11 (2017) 284–295. doi:10.1007/s11706-017-0391-y.
- [101] G.L. Song, *Corrosion of magnesium alloys*, 1st ed., Woodhead Publishing, 2011. doi:10.1533/9780857091413.
- [102] L.-Y. Li, B. Liu, R.-C. Zeng, S.-Q. Li, F. Zhang, Y.-H. Zou, H.G. Jiang, X.-B. Chen, S.-K. Guan, Q.-Y. Liu, In vitro corrosion of magnesium alloy AZ31 — a synergetic influence of glucose and Tris, *Front. Mater. Sci.* 12 (2018) 184–197. doi:10.1007/s11706-018-0424-1.
- [103] M. Ascencio, M. Pekguleryuz, S. Omanovic, An investigation of the corrosion mechanisms of WE43 Mg alloy in a modified simulated body fluid solution: The influence of immersion time, *Corros. Sci.* 87 (2014) 489–503. doi:10.1016/J.CORSCI.2014.07.015.
- [104] W.-D. Mueller, M. Lucia Nascimento, M.F. Lorenzo de Mele, Critical discussion of the results from different corrosion studies of Mg and Mg alloys for biomaterial applications, *Acta Biomater.* 6 (2010) 1749–1755. doi:10.1016/J.ACTBIO.2009.12.048.
- [105] R. Astala, M.J. Stott, First Principles Investigation of Mineral Component of Bone: CO<sub>3</sub> Substitutions in Hydroxyapatite, *Chem. Mater.* 17 (2005) 4125–4133. doi:10.1021/CM050523B.
- [106] S. Hiromoto, A. Yamamoto, High corrosion resistance of magnesium coated with hydroxyapatite directly synthesized in an aqueous solution, *Electrochim. Acta.* 54 (2009) 7085–7093. doi:10.1016/J.ELECTACTA.2009.07.033.
- [107] S. Höhn, S. Virtanen, A.R. Boccaccini, Protein adsorption on magnesium and its alloys: A review, *Appl. Surf. Sci.* 464 (2019) 212–219. doi:10.1016/J.APSUSC.2018.08.173.

### Figure captions

Fig. 1. Optical images of the SVET probe and SIET microelectrode, SEM image of the SVET probe tip, schematic of the SIET microelectrode tip and photo of the isolated surface with electrodes before SVET/SIET tests.

Fig. 2. Schematics of the solution circulation through the SVET/SIET cell (a) and hydrogen evolution test with flow-through cell (b), which show the direction of the flow (MEM was used as an example).

Fig. 3. Optical images of the investigated area (limited by frame) (a) before exposure (1), after 24 (2), 48 (3) and 70 (4) h of the sample exposure to 0.83 % NaCl solution as well as SVET (b) and SIET (c) maps after 2 (1), 24 (2), 48 (3) and 70 (4) h of the sample exposure.

Fig. 4. Optical images of the investigated area (limited by frame) (a) before exposure (1), after 24 (2), 48 (3) and 70 (4) h of the sample exposure to MEM solution as well as SVET (b) and SIET (c) maps after 2 (1), 24 (2), 48 (3) and 70 (4) h of the sample exposure.

Fig. 5. The evolution of the sum of total cathodic and anodic currents (a) as well as the separate total anodic (b) and cathodic currents evolution (c) for the MA8 magnesium alloy sample in MEM and 0.83 % NaCl solutions. Trend line (dotted line) was used to describe the corrosion evolution.

Fig. 6. The evolution of anodic (a) and cathodic current density peaks (b) for the MA8 magnesium alloy sample in MEM and 0.83 % NaCl solutions.

Fig. 7.  $\text{pH}_{\text{max}}$  and  $\text{pH}_{\text{min}}$  (a),  $\Delta\text{pH}$  (b) and bulk pH (c) evolution during 70 hours of sample exposure to MEM and 0.83 % NaCl solutions. Trend line (dotted curve) was used to describe the corrosion of MA8 Mg alloy sample.

Fig. 8. Normalized hydrogen evolution rate diagram (a) coupled with daily measurements of the bulk pH (b) for MA8 magnesium alloy samples in MEM and 0.83 % NaCl solutions during 30 days. Trend line (dotted line) was used to describe the corrosion of MA8 Mg alloy sample. The pH evolution of MEM in the absence of Mg alloy during 10 days (c).

Fig. 9. Normalized hydrogen evolution rate diagram for MA8 magnesium alloy samples in MEM during 7 days in unsterile conditions (the upper curve) and in sterile ones (the lower curve).

Fig. 10. Normalized hydrogen evolution rate diagram coupled with daily measurements of the bulk pH of the solution for MA8 magnesium alloy samples in MEM during 100 h. Tests were carried out using flow-through cell.

Fig. 11. XRD patterns of the MA8 Mg alloy after 30 days of exposure to 0.83 % NaCl (a) and MEM (b). The detailed XRD characterization of the corrosion film formed on MA8 Mg alloy after 30 days in MEM (c).

Fig. 12. SEM images and corresponding EDX spectra of the corrosion product film (areas 1, 2, 3) formed on MA8 Mg alloy after immersion in 0.83 % NaCl solution (1a, 1b) and in MEM (2a, 2b; 3a, 3b) for 30 days.

Fig. 13. SEM image (a) of the film formed on the MA8 Mg alloy after immersion in MEM solution for 30 days and corresponding EDX maps (b-f) of the elements (C, Ca, P, Mg, O) distribution in this area.